Analysis of the Contact Stresses of Spur Gears Manufactured by 3D Printing from Composite Materials

Milan Zmindak[0000-0001-6426-8493], *Michal* Kaco[0000-0003-0840-7043], and *Alzbeta* Sapietova[0000-0001-8489-0853]

Department of Applied Mechanics, Faculty of Mechanical Engineering, University of Zilina, Univerzitna 1, 01026 Zilina, Slovakia

Abstract. Additive manufacturing is a technology rapidly expanding on a number of industrial sectors. However, it is still hampered by low productivity, poor quality and uncertainty of final part mechanical properties. Materials for production of given components are composite materials, especially on the basis of so-termed CFRP, CRP (carbon fibre - so-termed polymers reinforced by carbon fibres). Composite fibers have properties that can add high strength and stiffness to the printed part. Like all manufacturing processes, composite printing is only suitable for certain design applications. The fibers have a predetermined width during printing and, due to geometrical limitations, can only be used to reinforce structures meeting a certain minimum thickness. The objective of this paper is to predict the contact stresses of carbon/onyx spur gear using Finite Element Analysis (FEA) results through the torque load. Finite element software ANSYS Workbench 20.0 is used to study the stress intensity factor of spur gear. A 3D solid model has been established for simulation of the spur gear which enables to understand the mechanical strength and strain at failure of the composite materials.

1 Introduction

The gear drive transmits power with comparatively smaller dimensions, light weight, less stress, runs reasonably free of noise and vibration with least manufacturing and maintenance cost [1-3]. Spur gear is a cylindrical shaped gear in which the teeth are parallel to the axis. Spur gears are easy to manufacture and it is mostly used to transmit power from one shaft to another shaft up to certain distance & it is also used to vary the speed & Torque. e.g. watches, gearbox etc. They form vital elements of main and ancillary mechanisms in many machines such as automobiles, tractors, metal cutting machine tools etc. Toothed gears are used to change the speed and power ratio as well as direction between input and output.

Composite materials are widely used in various industries. It is well known that their main advantages are very good mechanical properties, chemical resistance, lower material consumption and low product weight [4, 5]. From an economic point of view, the main disadvantage of composite materials is their relatively high price. The properties of composite materials often depend on the position and direction of their individual

components in a fixed coordinate system. In the mechanics of flexible bodies, these materials are referred to as heterogeneous and anisotropic. These materials consist of two or more components, which usually have different material properties. The supporting part of the composite are reinforcing fibers (long or short, eventually particles), the connecting element being a matrix. Fiber composites and laminates are represented at the macro level of homogenized substances with an equivalent or effective modulus of elasticity.
The trend of recent years is the production of composite materials using 3D printing technology weight [6]. The principle of 3D printing is to gradually add material layer by layer. There are several technologies for 3D printing, but fusion deposit modeling (FDM) and continuous fiber production (CFF) technologies are most commonly used for composite printing [7]. For example, the MarkTwo 3D printer, co. Markforged (which will also be used to make test samples) has two print nozzles. One nozzle is used to print material from a nylon or onyx matrix, the other nozzle is used to print a reinforced fiber. The reinforced fiber is coated with nylon or onyx. Fibers of various materials are available (kevlar, glass fiber, carbon fiber) [8].
In this paper, MarkTwo3D printer, manufactured by Markforged[9] has been the ALM/FDM system used to produce a spur gears. The contact stress are analyzed through the FEM for steel and composite spur gear. Finally FE model with a segment of three teeth is considered for crack propagation using SMART (Separating- Morphing-Adaptive and Remeshing Technology) Crack-Growth method.

2 3D printing technique of gears

3D printing is an additive part manufacturing process that is different from traditional manufacturing techniques as is machining, casting and forming [10]. Additive production is controlled by automated systems. Physical 3D models are made from computer models using metallic plastic, ceramic materials. Composite gears have better mechanical characteristics like wear resistance, corrosion resistance, lubricant free, noiseless high strength to weight ratio, etc..

2.1 Markforged and Eiger

Markforged 3D printer was used for printing spur gears (Fig.1). The material used in the Markforged 3D printer contains an Onyx matrix. The material Onyx is produced from hard nylon, which provides a stiffness equal to or greater than any pure thermoplastic used to create products on a 3D printer.The Onyx filament contains chopped micro-carbon fibers, combing thetoughness of nylon and thermal properties of carbon[11]. Thiscomposite filament provides a dimensionally stable, stiff, andheat tolerant engineering material with high quality surface finish. The Onyx is suitable for customers who require high demands on the visual side of the product. Surface quality exceeds the properties of plastic 3D prints made, for example, from PLA (Polylactic acid) material.

Fig. 1. Markforged 3D printer.

2.2 Fiber reinforcement

The most important rule for the fiber path at gears is the rule that applies to teeth. A gear printed on a 3D printer needs to have the reinforced fibers located in its teeth, as this is the most critical location for pitting damage (Fig.2).In order for the tooth of a gear to be properly reinforced with fiber all the way from the root to the tip, it must be wider than the minimum 3.8 mm threshold at the tip of thegear tooth.The minimum part width for a thin region connected to a larger part at both ends is 2.9 mm [12].

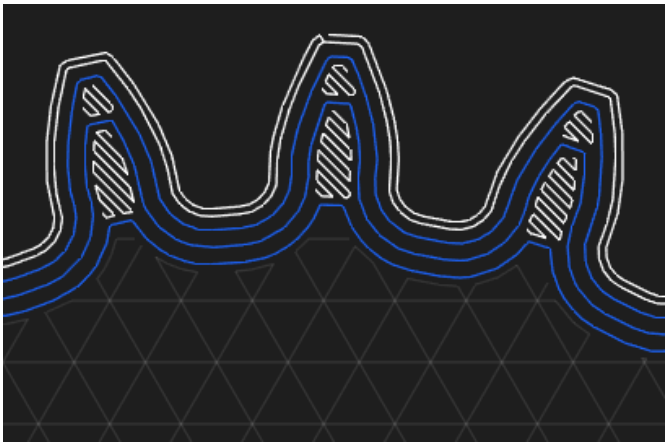

Fig. 2. Reinforcement of gearing from the root to the tip of the tooth.

In the case of smaller gears, fiber can often help reinforce the tooth, but may not be able to fit all the way to the tip. This will still result in a gear that is stronger than a pure plastic one, but be weaker locally long the tooth than desired. In this case fiber reinforcement can only reach slightly beyond the pitch circle of the gear.

3 Finite element modeling and simulation

Finite element method (FEM) is particularly interesting for modelling 3D printed part due to its flexibility in analyzing complex geometries in both macro and micro scale [13,14]. A very important parameter when designing a gear pair is the maximum contact stress that exists between two gear teeth in mesh, as it affects surface fatigue (namely. pitting and wear) along with gear mesh losses, A lot of attention has been targeted to the determination of the maximum contact stress between gear teeth ill mesh, resulting in many "different" formulas. Moreover, each of those formulas is applicable to a particular class of gears (e.g, hypoid, worm. spiroid, spiral bevel or cylindrical-spur and helical) [15-18].
More recently, FEM has been introduced to evaluate the contact stress between gear teeth. Presented below is a single methodology for evaluating them a maximum contact stress that exist between gear teeth in mesh.FEM software. ANSYS allows specify the required boundary conditions to the composite model, input values for composite dimensions and material properties of the composite, etc. [19-21].

3.1 Spur gear geometry

Spur gears are used to transmit power between parallel shafts. The Fig. 3 shows a pair of identical spur gears. In Fig. 4 is shown the basic spur gear geometry. Spur gears have their teeth cut parallel to the axis of the shaft on which the gears are mounted. To maintain a constant angular velocity ratio, two gears must satisfy a fundamental law of gearing: the shape of the teeth must be such that *the common normal* (8) at the point of contact between two teeth must always pass through a fixed point on *the line of centers* (5). This fixed point is called the *pitch point* (6). The angle between the line of action (8) and the common tangent of the pitch circles (7) is known as the *pressure angle*. The parameters defining a spur gear are its pitch radius r_p, *pressure angle* ($\alpha = 20^0$) and number of teeth (N). The teeth are cut with a radius of addendum r_a (9) and a radius of addendum r_d(10). The shaft has a radius r_s(11) and the fillet radius is r_f (12). The thickness of the gear is 20.0 mm. The spur gears parameters are used form [22] and are given in Table 1.

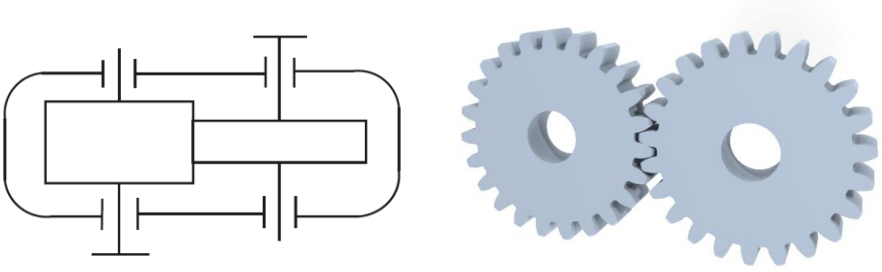

Fig. 3. A pair of gears.

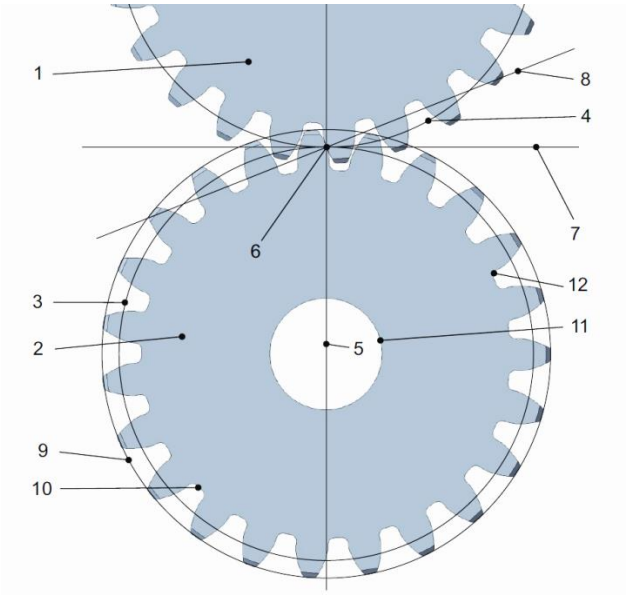

Fig. 4. Basic spur gear geometry.

1 - the driving gear rotates clock wise, 2 - the driven gear rotates, 3 - pitch circle, 4 - pitch circle of the driving gear, 5- line of centers, 6 - contact point (pitch point), 7 - common tangent of the pitch circles, 8 - line of action (common normal of contacting gears), 9 - addendum, 10 - dedendum, 11 - shaft, 12- fillet

Table 1. Dimensions of the spur gears.

Dimensions	Symbol	Value
Shaft centre distance [mm]	a	91.5
Effective face width [mm]	b	20
Working pitch diameter [mm]	d_w	91.5
Tip diameter [mm]	d_a	99.89
Module [mm]	m	4
Number of teeth [-]	N	23
Profile shift coefficient [-]	x	-0.061
Pressure angle [°]	α	20
Working pressure angle [°]	α_w	19.12
Overlap ratio [-]	ε_α	1.69

3.2 Boundary conditions

First of all, we have prepared assembly in Creo Parametric for spur gear and save as this part as IGES for Exporting into ANSYS Workbench Environment [23]. Based on the

assumptions of Lewis equation, the boundary conditions are set in ANSYS Workbench. The fixed support is used at the root end of the tooth and the Z component of the moment is applied, red colour (Fig.5).

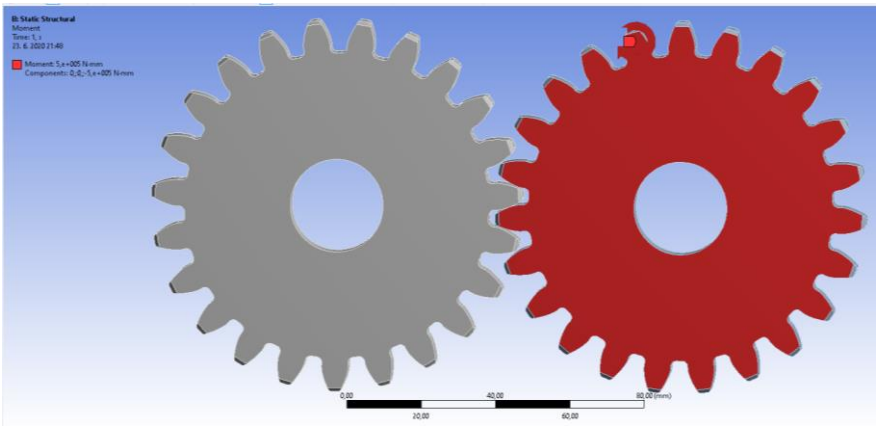

Fig. 5. Boundary conditions.

3.3 Meshing

Meshing is basically the division of the entire model into finite elements so that at each and global the stiff equations are solved. The number of elements and the type elements significantly affects the accurate of solution and also improves the quality of solution. In our case quality, the quality of the mesh is controlled by the choice adaptive sizing and mesh defeaturing. The target quality is 0.05 and transition ratio is 0.272. The maximum layers are 5 and growth rate is 1.2. Here the element size of 1 mm with medium smoothing is considered for mesh generation (Fig.6). The geometry is created by 49 faces, number of nodes is 106868 and number of elements is 59727. The contact is frictional, number contacting is 23, penetration is 6.3968e-04, geometric penetration is 6.3968e-04, geometric gap is 4.0283e-05 and resulting pinball is 0.9126.

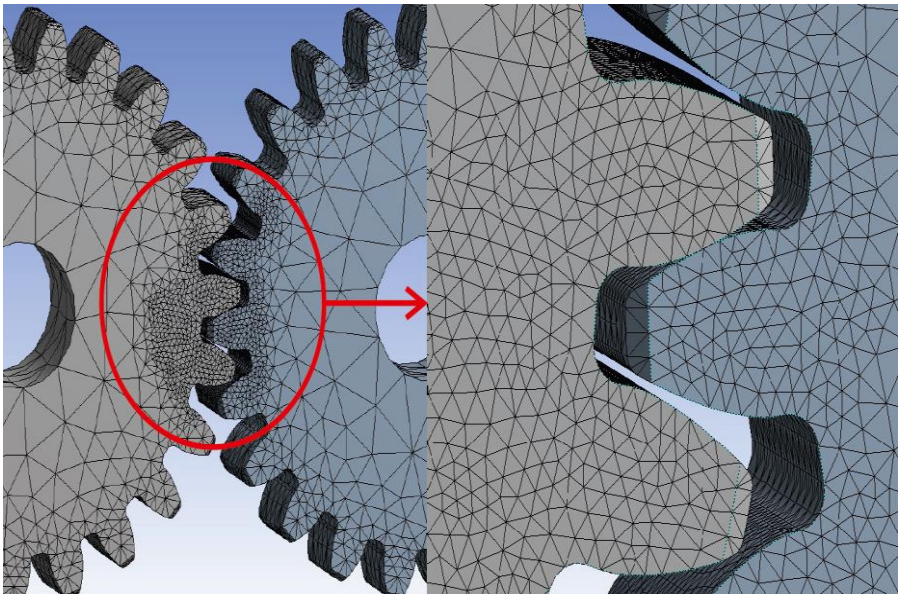

Fig. 6. FEM mesh.

3.4 Frictional model

In the basic Coulomb friction model, two contacting surfaces can carry shear stresses. When the equivalent shear stress is less than a limit frictional stress ($\tau_{lim}\tau$), no motion occurs between the two surfaces [24]. This state is known as sticking. The Coulomb friction model is defined as:

$$\tau_{lim} = \mu p + b \tag{1}$$

$$\|\tau\| \leq \tau_{lim} \tag{2}$$

where

τ_{lim} − limit frictional stress

$\|\tau\| - \begin{cases} |\tau| \text{ equivalent stress fro 2D contact} \\ \sqrt{\tau_1^2 + \tau_2^2} \text{equivalent stress for 3D contact} \end{cases}$

μ −coefficient of friction for isotropic friction

p −contact normal pressure

b−contact cohesion

Once the equivalent frictional stress exceeds τ_{lim} the contact and target surfaces will slide relative to each other (Fig. 7). This state is known as sliding. The sticking/sliding calculations determine when a point transitions from sticking to sliding or vice versa. The contact cohesion provides sliding resistance even with zero normal pressure. The coefficient of friction 0.2 was specified for our case.

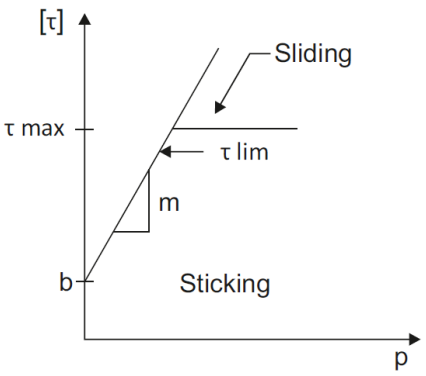

Fig. 7. Friction model.

3.5 Material

Selecting different materials for gears plays an important role in gear technology. Material selected for making a gear must satisfy two conditions: (1) manufacturability and processing requirement: (2) achieving required service life. Manufacturability requirement includes its forgeability and its response to heat treatment. Whereas, to achieve required service life, gears should transmit power to a satisfactory level when working in loading conditions as well as fulfilling mechanical property requirement such as fatigue, strength and response to heat treatment.
The material used for this analysis is Onyx matrix reinforced by carbon fibres. Material properties of both materials are given in Table 2 and Table 3. Homogenized material properties for volume fraction of gear teeth $v_f = 0.4$ are given in Table 4.

Table 2. Material properties of Onyx.

Material	Modulus of elasticity (E) [GPa]	Poisson´s ratio (μ)	Density (ρ) [g/cm^3]
Onyx	1.4	0.3	1.2

Table 3. Material properties of carbon fiber.

Material property	Value
Modulus of elasticity of lamina in the direction of fibersE_1 [GPa]	64.7
Transverse modulus of elasticity E_2 [GPa]	22.4
Shear modulus of elasticity of the lamina G_{12} [GPa]	22.1
Shear modulus of elasticity of the lamina G_{23} [GPa]	8.3
Poisson´s ratio μ_{12}	0.3
Poisson´s ratio μ_{23}	0.35
Density ρ [g/cm^3]	1.4

Table. 4. Homogenized material properties of unidirectional composite.

E_{11} [GPa]	E_{22} [GPa]	E_{33} [GPa]	ν_{12} -	ν_{13} -	ν_{23} -	G_{12} [GPa]	G_{13} [GPa]	G_{23} [GPa]	ρ [kgm-^{3}]
5.960	1.501	1.501	0.30	0.30	0.4	4.369	3.902	3.902	1490

4 Numerical results

Fig. 8 shows thevon Mises stress contour for steel spur gears and Fig.9 for material onyx + carbon. The maximum values of von Mises stress are 59.28 MPa for material steel and 99.35 for material onyx + carbon. The next FEA results are compared in Table 5.

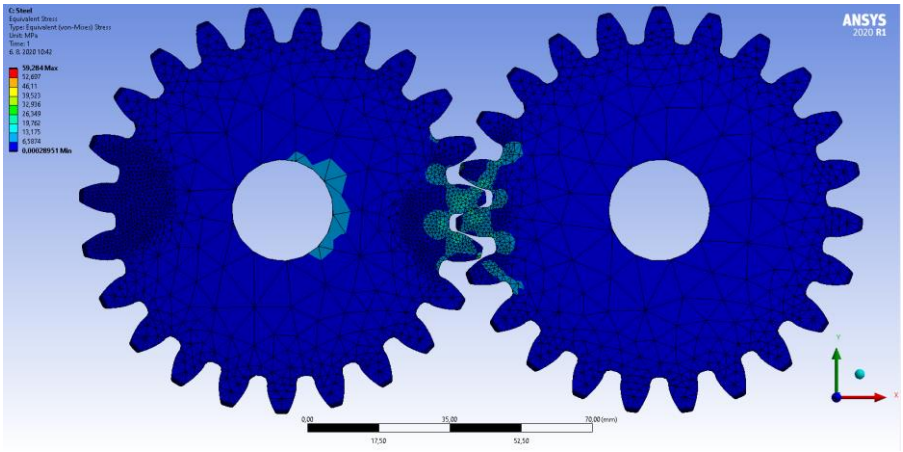

Fig. 8. Von Mises stress (steel).

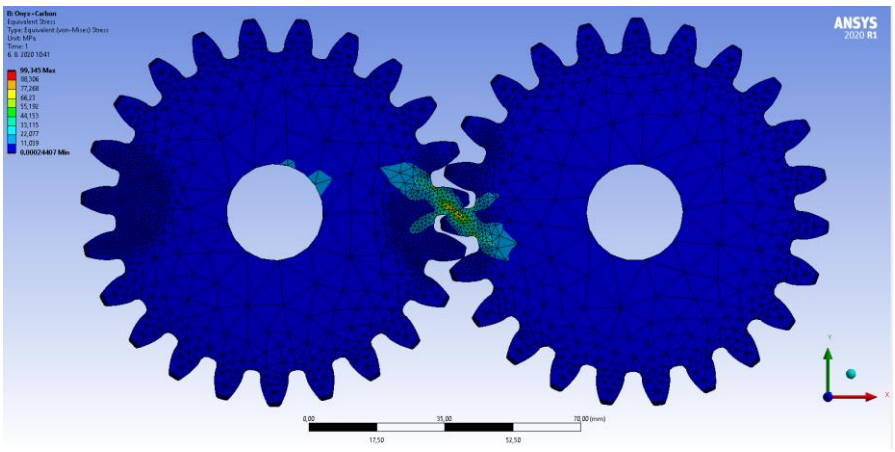

Fig. 9. Von Mises stress (onyx + carbon).

Table 5. Simulation results.

	Structural steel	Onyx + Carbon
von Mises stress [MPa]	59.28	99.35
Contact pressure [MPa]	67.55	83.77
Friction stress [MPa]	0.43	11.08
Sliding [mm]	$12.26*10^{-5}$	$720.14*10^{-5}$
Penetration [mm]	$24.7*10^{-5}$	$1825*10^{-5}$

5 Fracture mechanics

Fracture mechanics mainly used for predicting strength and life of cracked structures. Using the computational methods of applied mechanics, the stress and deformation states at the crack are determined. Linear elastic fracture mechanics can be used to describe the behaviour of cracks. The basic assumption of this theory is determining the crack growth behaviour in elastic domain of material by using stress intensity factors (SIF). Therefore, calculating the SIFs is very important to achieve accurate results [25].
Fracture analysis is typically accomplished using either the energy criterion or the SIF criterion. For the energy criterion, the energy required for a unit extension of the crack (the energy-release rate) characterizes the fracture toughness. For the SIF criterion, the critical value of the amplitude of the stress and deformation fields characterizes the fracture toughness. Under some circumstances, the two criteria are equivalent [26].
We note that the fracture toughness of composites, made by combining engineering polymers, with greatly exceeds the individual fracture toughness of the constituent materials.
Computational methods for evaluating the fracture parameters can be broadly categorized as[27]:

- Methods wherein the singular fields near the crack tip or crack front are modeled explicitly by spatial discretization schemes such as finite element methods (FEM) or boundary element methods (BEM).
- Superposition methods wherein the singular fields are treated entirely analytically (through infinite body solutions), and spatial discretization techniques are employed to solve only the uncracked structure.

The FEM has been successfully used to compute the SIFs in stress analysis of crack problems with finite domains and general, complex boundary conditions, for which analytical solutions are not available. When conventional, conforming displacement elements are used, the stress singularities developing at the tin of a crack or at the tree of a tinted crack are modeled either through suitable geometric transformations of by adopting appropriate interpolation functions. In general, the computation of SIFs is performed indirectly and requires the use of highly refined finite element meshes in the neighborhood of the crack to shape with accuracy the characteristics high stress gradients developing locally. Static and dynamics linear and nonlinear fracture mechanics analysis can be performed with many commercials software for example ADINA, ANSYS, MARC etc.
The SIF is one of the most important and currently also the most used mechanical quantities describing the state of stress in a cracked body. This parameter includes both the size and method of external loading, as well as the basic qualitative and quantitative characteristics of the geometry of the body and the crack.

The SIFs describe the magnitude of the elastic stress field at a crack front. The SIF in general is mainly dependent on load, crack length

$$K = f\left(load, crack\ length, geometry\right) \tag{3}$$

The stress fields in any linear elastic cracked body are expressed as[28]

$$\sigma_{ij} = \left(\frac{K}{\sqrt{2\pi r}}\right) f_{ij}\left(\theta\right) + \sum_{m=0}^{\infty} A_m r^{\frac{m}{2}} g_{ij}^{(m)}\left(\theta\right) \tag{4}$$

where σ_{ij} are the Cauchy stresses, r is distance from the crack and θ is the angle with respect to the plane of the crack (Fig. 10), f_{ij} is a dimensionless functions of θ which is dependent on the geometry of crack and loading conditions For the higher-order terms, A_m is amplitude and is a dimensionless function of θ for*m*th*term*. These equations apply to any of the three fracture modes (opening mode, shearing mode, tearing mode). Since the quantity f_{ij} is dimensionless, the SIF can be expressed in unitsof $MPa\sqrt{m}$.

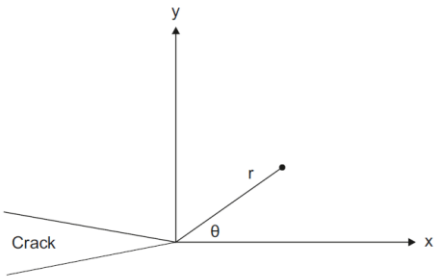

Fig. 10. Schematic of a crack tip.

For linear elastic problems, the displacements near the crack tip (or crack front) vary as $1/\sqrt{r}$. The stresses and strains are singular at the crack tip, varying as

$$\sigma_{ij} = -\frac{K}{\sqrt{r}} f_{ij}\left(\theta\right) \tag{5}$$

$$\varepsilon_{ij} = -\frac{K}{\sqrt{r}} g_{ij}\left(\theta\right) \tag{6}$$

To produce this singularityin stresses and strains, the crack tip mesh should have certain characteristics:A mesh of circular rings of elements near the crack tip is needed,the quarter-point element is widely used in linear elastic fracture computations with the FEM. In this case the shape functions contain singular crack-specific functions the free parameters of which are related to the *K* factors. Special elements of this type are called crack tip elements (CTE) (Fig.11). They are utilized to discretize the direct surroundings of the crack tip, while regular elements are then used to model the rest of the structure.

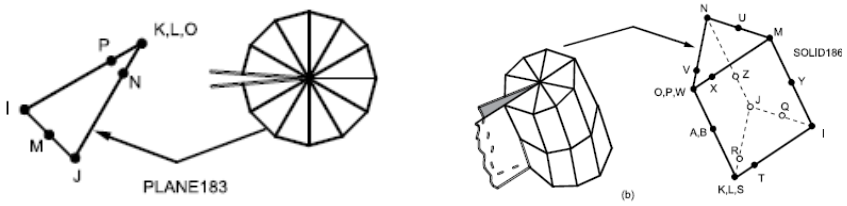

Fig. 11. Singular elements.

5.1 Orthotropic mixed mode fracture and SIF calculation

An orthotropic composite material behaviour can be further idealized in order to simplify the process of crack modelling; a fibre composite structure is assumed as a homogeneous orthotropic continuum, where the crack growth takes place in an idealized material with anisotropic constituents. In this approach, the details of local failures of the composite, such as broken fibres or cracked matrix, are not considered and an equivalent orthotropic continuum is adopted [29].

SIF Calculation by Interaction Integral

The SIF is one of the important parameters representing fracture properties of a crack tip. The domain integral method is adopted to evaluate the mixed modes tress intensity factors in homogenous orthotropic media

$$J = \int_{\Gamma} \left(w_s \delta_{1j} - \sigma_{ij} \frac{\partial u_i}{\partial x_1} \right) \mathbf{n}_j \, d\Gamma \tag{7}$$

where $w_s$is the strain energy density for linear elastic material, $\delta_{1j}$is the Kronecker delta, Γ is an arbitrary contour around the crack tip which encloses no other cracks or discontinuities and over which the integration is carried out, $\mathbf{n}_j$ is the jthcomponent of the outward unit normal to Γ, and $\mathbf{u}_i$is the component of the displacement vector. Eq. (5) is not well suited for the finite element solutions, and an equivalent form of the J integral can be obtained by exploiting the divergence theorem in the form of the domain integral approach

$$J = \int_{A} \left(\sigma_{ij} - \frac{\partial u_i}{\partial x_1} w_s \delta_{1j} \right) \frac{\partial q}{\partial x_j} dA \tag{8}$$

where A is an area surrounding the crack tip (the interior region of Γ) and q is a smoothly varying function. Γ is usually assumed as a circular or rectangular area whose center locates on the crack tip.

The extended finite element method (XFEM) to overcome the singularity, $1/r$ problems at the crack tip by incorporating the singularities in local approximation. The XFEM is based on enriching the degrees of freedom in the modelwith additional displacement functions that account for the jump in displacements across the cracksurface.The method is used to propagate cracks in linear elastic materials based on user-specifiedfracture criteria. With SMART (separating morphing and adaptive remeshing technology) fracture modeling functionality in ANSYS Mechanical, crack growth analysis is not dependent on the mesh. Fracture modeling is faster and more accurate, and requires much less special expertise. For more information, see XFEM-Based Crack Analysis and Crack-Growth Simulation [26]

The approach for evaluating the energy-release rate is based on the virtual crack-closure technique (VCCT). VCCT is based on the assumption that the energy needed to separate a surface is the same as the energyneeded to close the same surface. The implementation described here uses the modified crack-closuremethod (a VCCT-based method) and assumes further that stress states around the crack tip do notchange significantly when the crack grows by a small valueof crack length (Δa).
The VCCT method for energy-release rate calculation supports the following material behaviors:linear isotropic elasticity, orthotropic elasticity, anisotropic elasticity

Fracture criteria

To model the crack growth, it is necessary to define a fracture criterion for crack onset and the subsequentcrack growth. For linear elastic fracture mechanics (LEFM) applications, the fracture criterion is generallyassumed to be a function of Mode I (GI), Mode II (GII), and Mode III ((GIII) critical energy-release rates,expressed as:

$$f = f\left(G_I^c, G_{II}^c, G_{III}^c, G_I, G_{II}, G_{III}, \cdots\right) \tag{9}$$

Fracture occurs when the fracture criterion index is met, expressed as:

$$f \geq f_c \tag{10}$$

where G_T^c is the fracture criterion ratio.The recommended ratio is 0.95 to 1.05. the default is 1.0.

Critical Energy-Release Rate Criterion

The critical energy-release rate criterion uses total energy-release rate (GT) as fracture criterion.Thetotal energy-release rate is summation of the Mode I (GI), Mode II (GII), and Mode III ((GIII) energy-releaserates, expressed as:

$$f = \frac{G_T}{G_T^c} = \frac{G_I + G_{II} + G_{III}}{G_T^c} \tag{11}$$

where is the critical energy-release rate.

Therefore, the SIFat the crack tip is studied to indicate the behavior of crack propagation towards the remote stress applied, especially on the strength of the cracked gear tooth [30].

5.2 Numerical results

In this section we will present some results using SMATR modelling in ANSYS Workbench software. Only a finite element model with a segment of three teeth is considered for analysis. Zero displacements and rotations (fixed support) are prescribed on the lower surface of the gear.Here the element size of 2 mm with medium smoothing is considered for mesh generation
The course of the von Mises stress is shown in the Fig. 12 and its maximum value is 855.98 MPa.The SIF was determined from the finite element nodal displacements and forces using J-integral method. A local coordinate system is defined for the crack tip. The components indicate crack propagation direction (x) and crack opening direction (y).Mode I loading refer to loads applied normal to the crack plane, which tends to open the crack.Mode II

refers to in plane shear loading. We select three named geometric regions to define the crack. These are the crack edge, the top surface of the crack and the bottom surface of the crack.

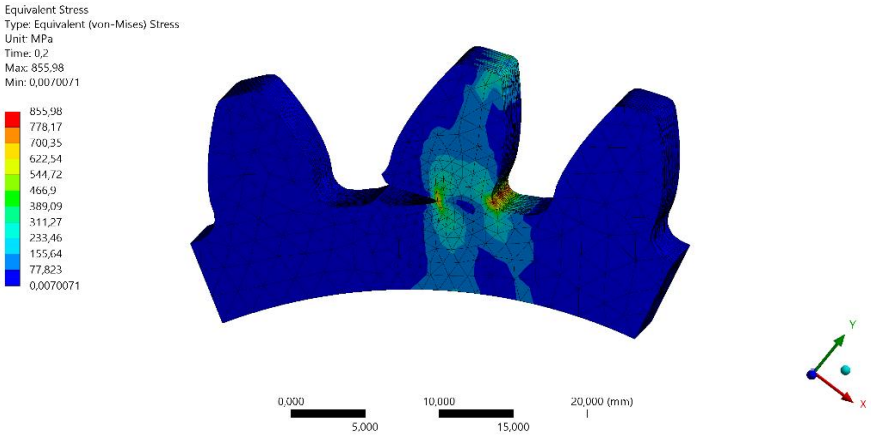

Fig. 12. Von Mises stress.

Each of these regions is then associated with a node set for use in the analysis. The top surface of the crack and the bottom surface of the crack has prescribed displacements 8 mm for X and Y components.Options for crack growth are: Initial crack is defined as pre-meshed crack, failure criteria option is SIF and critical rate is 6.3246e-05 MPa.mm$^{1/2}$ and element size is 2 mm.

SIF for crack propagation under static load is shown in the Fig. 13 and its maximum value is -86.71 MPa.mm$^{1/2}$. We see that its value is negative. In physical sense, the negative mode I SIF is incorrect. When the crack is within a compressive stress field, the negative mode I SIF often occurs. The negative mode II stress intensity factor is attributed to the direction of the tangential component (shear) of the applied load in the mixed mode conditions.

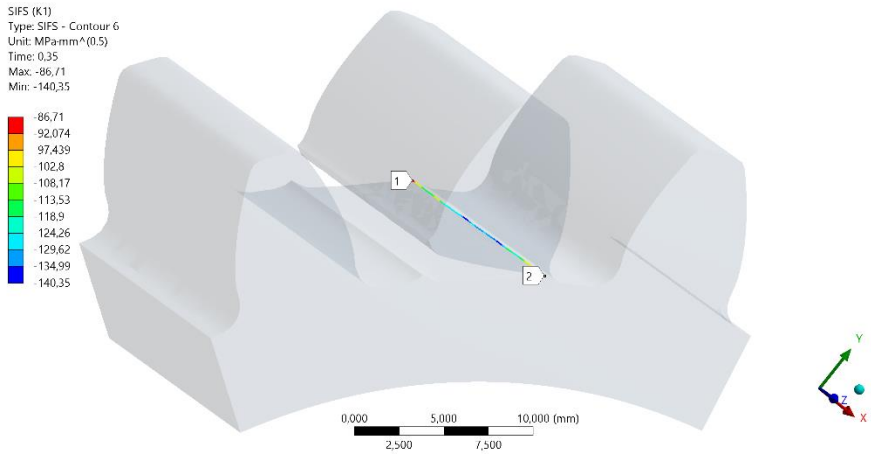

Fig. 13. SIF- Contour 6.

The graph plots the distance of the crack front node from the origin and the energy release rate as it moves along the crack front.The number of solution contours is set to 6. These are the "loops" through the mesh around the crack tip, which are used to evaluate the SIF by integrating the crack tip region strain energy. The fracture mechanics approach avoids the stress singularities at the crack tip in the analysis.
The curvesin Fig. 14present the six contours (cont 1 to cont6) requested in the Pre-Mesh Crack object. They are used to check for convergence of the KI value. The first red curve is from a contour close to the crack tip; the other curves represent contours at increasing distances. The curves converge quickly, showing the mesh is adequate.

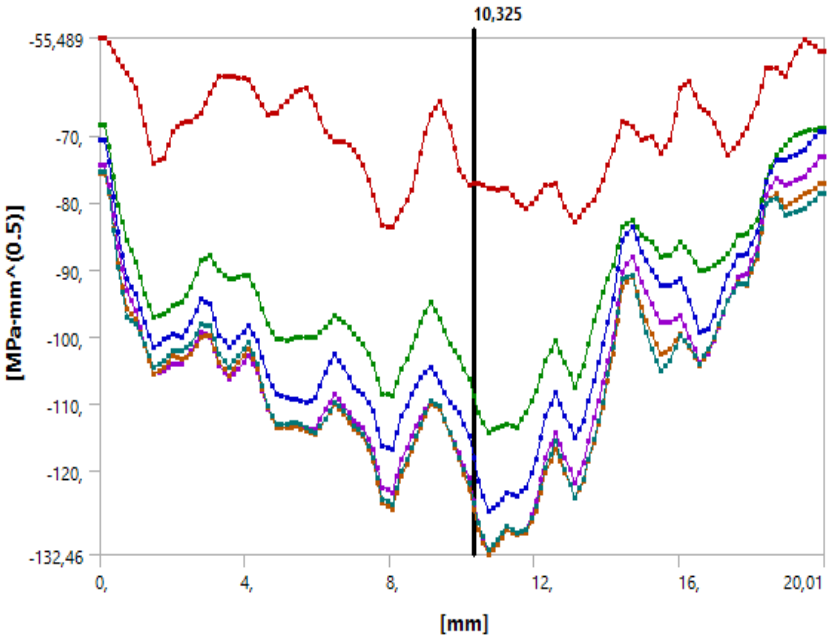

Fig. 14. SIF- Contour 6.

The meaning of colours: cont 1-red, cont 2-light green, cont 3 - blue, cont 4 – purple, cont 5- orange, cont 6, dark green.

6 Conclusions

In this paper, a 3D deformable-body (model) of spur gears is developed. This study provides a foundation for future studies on calculation of contact stresses and SIF for crack propagation under static load using FEM. The model is applied onto commercial FEA software ANSYS Workbench. A general finite element model was developed for evaluating the contact stress and SIF in spur gears ofequal geometry in both gears.From the result it could be concluded that the von Mises stressand contact pressure of composite material is slightly larger compared to steel.Friction stress is very larger for composite materials with friction coefficient 0.2.
Finite element analysis has been carried out for gear crack propagation. SIF for crack propagation under static load was calculated.We see that its values are negative.This is probably due to the crack is within a compressive stress field.

Acknowledgments

This work was supported by the Scientific Grant Agency of the Ministry of Education of Slovak Republic and the Slovak Academy of Sciences under Projects VEGA 1/0141/20 and VEGA 1/0510/20

References

1. F.L. Litvin Theory of Gearing. Cambridge University Press (1989).
2. S.P. Radzevich Theory of Gearing, Kinetics, Geometry, and Synthesis. CRC Press, Boca Raton (2012).
3. P. Lynwander Gear driven systems, Design and applications. Marcel Deker(1983).
4. E.J. Barbero Introduction to Composite Materials Design, Boca Raton, CRC Press (2011)
5. H. Altenbach, J. Altenbach, W. Kissing Mechanics of Composite Structural Elements. Berlin, Springer - Verlag (2004).
6. T.D. Ngo, A. Kashani, G. Imbalzano, T.Q.K. Nguyen, D. Hui, D Additive manufacturing (3D printing): A review of materials, methods, applications and challenges. Composites Part B 143, 172-196 (2018).
7. J.M. Chacon, M.A. Caminero, E. García-Plaza, P.J. Nunez Additive manufacturing of PLA structures using fused deposition modelling: Effect of process parameters on mechanical properties and their optimal selection. Materials and Design 124, 143-157 (2017).
8. D. Bourell, J.P. Kruth, M. Leu, G. Levy, D. Rosen, A.M. Beese, A. Clare Materials for additive manufacturing. CIRP Annals-Manufacturing Technology 66, 659-681 (2017).
9. https://markforged.com - access 21.02.2022.
10. S. Killi (Ed.) Additive Manufacturing: Design, Methods, and Processes. Pan Stanford Publishing Pte. Ltd. (2017).
11. S. Rajeshkumar, R. Manoharan Design and analysis of composite spur gears using finite element method, IOP Conf. Series: Materials Science and Engineering 263 doi:10.1088/1757-899X/263/6/062048 (2017)
12. N. Sondej Threading the Needle with Ease: Minimum Fiber Feature Sizes.[online], Available on: https://markforged.com/blog/threading-the-needle-with-ease/ (2016)
13. P. Kopas, M. Saga, V. Baniari, V., M. Vasko, M. Handrik A plastic strain and stress analysis of bending and torsion fatigue specimens in the low-cycle fatigue region using the finite element methods. Procedia Engineering 177, 526-531 (2017).
14. T. Kotkar, P. Masure, P. Modake, Ch. Lad, P. Basanagouda Modelling and Testing of Spur Gear made of Different 3D Printed Materials. Int. J. of Scentific Research in Science 4(4), 2394-4099 (2018).
15. S. Bodzas Tooth contact analysis of helical gears having modified straight teeth by changing of the number of teeth on the pinion, Strojníckyčasopis - Journal of Mechanical Engineering, 70 (1), 1-16 (2020).
16. E.E. Dooner Design formulas for Evaluating Contact Stress in Generalized Gear Pairs. Gear Technology, 31-37 (2001).
17. A.R. Hassan Contact stress analysis for a pair of mating gears, World Academy of Science, Engineering and Technology 58, 611-616 (2009).
18. S.Ch. Hwang, J.H. Lee, D.H. Lee, D.H., S.H. Han, K.H. Lee Contact stress analysis for a pair of mating gears, Mathematical and Computer modelling 57, 40-49 (2013).
19. N.L. Min, M.P. Thu Stress analysis on spur gears using ANSYS Workbench 16. International Journal of Science and Engineering Applications, 7(8), 2319–7560, (2018).
20. V. Singh, S. Chauhan, A. Kumar Finite element analysis of a spur gear tooth insing ANSYS and stress reduction by stress relief hole. Int. J. of Emerging and Developments 6(2), 491-495 (2012).

21. M.P. Thu, N.L. Min Stress analysis on spur gears using ANSYS Workbench 16.0. Int. J. of Science and Engineering Applications (7/8), 208-213 (2018).
22. A. Dimic, Z. Miskovic, R. Mitrovic, R. et al. The influence of material on the operational chracteristics of spur gears manufactured by 3D printing technology. Journal of Mechanical Engineering – Strojníckyčasopis 68 (3), 261 – 270, (2018).
23. ANSYS Workbench user's Guide. Release 19.2, ANSYS Inc. (2018).
24. ANSYS Theory Reference. Release 19.2, ANSYS Inc. (2018).
25. M. Kuna, Finite Elements in Fracture Mechanics, Theory-Numerics-Applications. Springer (2013).
26. ANSYS Mechanical APDL Fracture Analysis Guide. ANSYS, Inc. (2020).
27. J. Sladek, V. Sladek, L. Jakubovicova Application of boundary Element Methods in Fracture Mechanics, MC Energy, Žilina (2001).
28. Anderson T.L. Fracture Mechanics: Fundamentals and Applications. CRC Press, Taylor &Francis Group, LLC (2017).
29. S. Mohammadi, XFEM fracture analysis of composites, Wiley (2012).
30. F.Z. Hiung, H.G. Al-Qrimli Implementation of XFEM in the study of gear crack propagation behaviour using the SIF on different moments. Int. J. Simulation and Process Modelling, 12, 3/4 (2017).